communications biology

A Nature Portfolio journal

Article

https://doi.org/10.1038/s42003-025-08880-5

Cryo-EM structure of the human Derlin-1/p97 complex reveals a hexameric channel in ERAD

Qian Wang[1,2,6], Deqiang Yao[3,6], Bing Rao[1,4,6], Ying Xia[2], Wenguo Li[2], Shaobai Li[2], Mi Cao[2], Yafeng Shen[2], An Qin[1,5] & Yu Cao[1,2]

The ER-associated degradation (ERAD) pathway retrotranslocates misfolded proteins from the ER lumen to the cytoplasm for proteasomal degradation. Derlin-1 and p97 are central to this process, forming a canonical 4:6 complex with tetrameric Derlin-1. Using cryo-electron microscopy, we identify a novel human Derlin-1/p97 complex with a 6:6 stoichiometry, where hexameric Derlin-1 assembles as three dimers. This hexameric channel forms a significantly larger trans-ER membrane tunnel, potentially accommodating bulkier substrates. Structural comparisons revealed conformational flexibility in Derlin-1, suggesting the "U"-shaped tetramer may act as an intermediate in hexamer formation. The formation of this hexameric channel is mediated by interactions with p97 and appears dependent on p97's ATPase activity, which provides the driving force for the transition between the tetrameric channel conformation to the intermediate "U"-shaped conformation. These findings highlight the dynamic nature of the Derlin-1/p97 complex and its implications for understanding ERAD retrotranslocation.

The Endoplasmic Reticulum (ER) plays a central role in protein synthesis, folding, and post-translational modifications, ensuring cellular proteostasis through a tightly regulated quality control system[1]. Proteins that fail to fold properly are targeted for degradation via the ER-associated degradation (ERAD) pathway, a process critical for cellular homeostasis[2,3]. ERAD, often activated by the unfolded protein response (UPR), identifies misfolded proteins within the ER lumen and facilitates their transport across the ER membrane back into the cytoplasm (retrotranslocation), where they are ultimately degraded by the proteasome[4–8]. Dysregulation of ERAD mechanisms can lead to the accumulation of misfolded proteins within the ER, contributing to numerous pathological conditions, including neurodegenerative diseases[9–12].

The ERAD process involves many protein factors, each orchestrating distinct steps from substrate recognition to cytoplasmic translocation and degradation[8,13–16]. Among these factors, the Derlin protein family and the AAA+ ATPase p97/VCP have emerged as central players in retrotranslocation, the pivotal step in which misfolded proteins are extracted from the ER membrane[15,17–19]. As members of the rhomboid superfamily, Derlin likely retains the unfolding activity due to conserved residues[20,21]. Yeast homologs of Derlin, Der1 and Dfm1, have been shown to induce membrane distortions, enabling substrate retrotranslocation[22,23]. Notably, Dfm1 shares a closer functional resemblance to human Derlin-1 (hDerlin-1) and is essential for coupling retrotranslocation with proteasomal degradation by regulating Cdc48, the yeast homolog of p97/VCP[24,25]. In mammals, Derlin-1 forms a tetrameric channel that allows for the extraction of substrate proteins[20,26]. Moreover, it recruits p97/VCP, assembling the retrotranslocation machinery[21,27]. Previous cryogenic electron microscopy (cryo-EM) studies revealed a retrotranslocation complex comprising Derlin-1 and p97/VCP in a 4:6 stoichiometry. In this configuration, p97 supplies the energy for retrotranslocation through ATP hydrolysis, while tetrameric Derlin-1 serves as a transmembrane channel, mediating substrate translocation. The interaction between the SHP box in the C-terminal domain of Derlin-1 (Derlin-1^{SHP}) and the N-terminal domain of p97 (p97^{NTD}) underpins conformational changes driven by ATP hydrolysis, which are critical for substrate translocation and degradation. Disrupting this Derlin-1^{SHP}-p97^{NTD} interaction has been shown to impair protein

[1]Department of Orthopaedics, Shanghai Key Laboratory of Orthopaedic Implant, Shanghai Ninth People's Hospital, Shanghai Jiao Tong University School of Medicine, Shanghai, China. [2]Shanghai Institute of Precision Medicine, Shanghai Ninth People's Hospital, Shanghai Jiao Tong University School of Medicine, Shanghai, China. [3]State Key Laboratory of Oncogenes and Related Genes, Ren Ji Hospital, Shanghai Jiao Tong University School of Medicine, Shanghai, China. [4]Department of Molecular and Cellular Physiology, Stanford University School of Medicine, Stanford, CA, USA. [5]Shanghai Frontiers Science Center of Degeneration and Regeneration in Skeletal System, Shanghai Ninth People's Hospital, Shanghai Jiao Tong University School of Medicine, Shanghai, China. [6]These authors contributed equally: Qian Wang, Deqiang Yao, Bing Rao. e-mail: yu.cao@shsmu.edu.cn

degradation, leading to the accumulation of misfolded proteins in both yeast and human cell models[24,28].

During retrotranslocation, the tetrameric Derlin-1 channel conforms to a "U"-shaped side-open state. This state is hypothesized to allow substrates to enter from the lipid environment or recruit additional ERAD factors. However, the molecular events following this conformational change remain poorly understood. In our study, we identified an unexpected role of Derlin-1 in stabilizing the "side-open" conformation by forming a non-canonical complex. Using cryo-EM, we resolved the structure of a Derlin-1/p97 complex in a 6:6 stoichiometry, where Derlin-1 hexamers associate with p97 hexamers. This novel "6-6" configuration suggests a more dynamic role for Derlin-1 in ERAD, possibly involving modulation of the structural integrity and functional dynamics of the retrotranslocation complex during substrate degradation.

Results

Cryo-electron microscopic analysis on human Derlin-1/p97 complex

Our previous cryo-EM studies demonstrated that a truncated form of human Derlin-1 (Derlin-1$^{\Delta 215\text{-}239}$) and p97 with an N-terminal truncation (p97$^{\Delta 1\text{-}20}$) assemble into a complex (hereafter referred to as the Derlin-1/p97 complex) consisting of four copies of Derlin-1 and six copies of p97[29]. However, in 2-D and 3-D classifications, we identified a subset of particles displaying a transmembrane domain (TMD) larger than that of the tetrameric Derlin-1, suggesting the existence of a higher oligomeric state of Derlin-1 (Supplementary Fig. 1). However, the suboptimal quality of EM signals in this particle subset precluded successful structural resolution. To enrich this higher oligomeric state, we introduced different nucleotide ligands to the sample, hypothesizing that p97 conformational changes might modulate the Derlin-1 channel and promote a "side-open" state, potentially enabling the recruitment of additional membrane components. Cryo-EM analysis of samples supplemented with ATP·BeF$_x$ indicated an increased abundance of the higher oligomeric Derlin-1/p97 complex. However, despite improved particle presence, attempts to generate a high-resolution map of the TMD component remained unsuccessful (Supplementary Fig. 1).

In contrast, supplementation with ADP·BeF$_x$ significantly enhanced the quality of the EM signals, enabling the identification of a class of particles with a well-resolved TMD region larger than that of tetrameric Derlin-1 in either a closed or open conformation. Further refinement and polishing yielded final EM maps with C3 symmetry at an overall resolution of 3.55 Å, with the core regions of Derlin-1 and p97 resolved to resolutions of 2.7 Å and 5.0 Å, respectively (Fig. 1, Table 1 and Supplementary Fig. 2). Molecular models were subsequently constructed using the Derlin-1 and p97 structures deposited in the Protein Data Bank (PDB ID: 7Y59) as templates.

Overall C-3 symmetry architecture of the heterododecameric Derlin-1/p97 complex

In previous studies, the canonical Derlin-1/p97 complex with a 4:6 stoichiometry (hereafter referred to as the Der-p97 4:6 complex) was characterized by cryo-EM[29]. In this complex, Derlin-1 forms a tetrameric channel (state A) or a "U"-shaped torn channel (state U) positioned atop the hexameric p97 ring. The structural mismatch between the C2 symmetry of Derlin-1 and the C6 symmetry of p97 resulted in symmetry-breaking within the complex (Fig. 2a, b). By contrast, the heterododecameric Derlin-1/p97 complex with a 6:6 stoichiometry (hereafter referred to as the Der-p97 6:6 complex) adopts an overall C3 symmetry, wherein the Derlin-1 and p97 hexamers share a common symmetry axis (Fig. 1a, b). Structural alignment of the Der-p97 6:6 complex with the 4:6 complex, using the p97 ring as a reference, revealed an approximate 12-degree tilt of the Derlin-1 hexamer relative to the Derlin-1 tetramer in the 4:6 configuration (inset, Fig. 2a).

While the p97 components of the complex resemble each other and have six near-to-identical inter-p97 interfaces, the Derlin-1 hexamer is formed through the trimerization of three dimers rather than the hexamerization of six Derlin-1 protomers. These dimers, designated as dimers i-iii, each consist of two subunits (e.g., A^i and B^i for dimer i) (Figs. 1b, 2a). The intradimer interface within Derlin-1 dimers exhibits close contact mediated

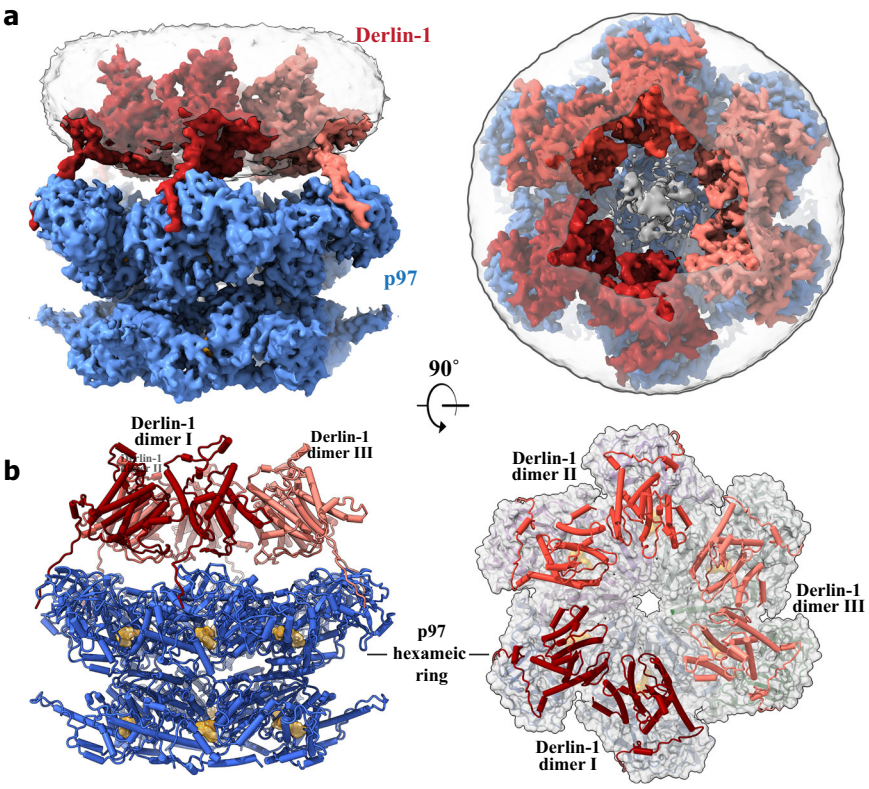

Fig. 1 | The overall architecture of the human Der-p97 6:6 complex. a The cryo-EM map of hexameric human Derlin-1 in complex with hexameric human p97. The cryo-EM map corresponding to p97 was shown in blue. The cryo-EM maps corresponding to the three groups of Derlin-1 dimers in the hexamer were colored dark red, red, and pink-red, respectively. The surrounding detergent/lipid layer is depicted as a transparent shell enveloping the Derlin-1 hexamer. **b** The structural model of the human Der-p97 6:6 complex. The Derlin-1 hexamer is displayed as a cartoon model, with dimers i-iii colored in dark red, red, and pink-red, respectively. The p97 hexamer is depicted as a cartoon model in blue (left) and as a surface model in gray (right). Nucleotide ligands bound to the p97 hexamer are represented as surface models in yellow. Both the cryo-EM map and structural model are presented in two views: parallel to the ER membrane (left) and from the lumen side of the ER membrane (right).

Table 1 | Cryo-EM data collection, processing, model refinement, and validation statistics

Data collection and processing	Der-p97 ADP·BeF$_x$ 6:6 complex (PDB: 9LLK EMDB-63205)
Microscope	Titan Krios G3i
Detector	Gatan K3 camera
Nominal magnification	81,000x
Voltage (kV)	300
Energy filter slit width	15 eV
Pixel size (Å/pixel)	1.1
Electron exposure (e^-/Å^2)	50
Defocus range (μm)	−1.0 to −2.5
Symmetry imposed	C3
Number of movies	11,785
Final particle numbers	129,127
Map resolution (Å)	3.55
FSC threshold	0.143
Map sharpening B factor (Å^2)	−103.2
Model building and refinement	
Model composition	
Protein Residues	5796
Ligands	12
R.m.s. deviations from ideal	
Bond lengths (Å)	0.004
Bond angles (°)	0.783
Validation	
All-atom clashscore	12.20
Rotamer outliers (%)	0.48
Ramachandran plot	
Favored (%)	90.47
Allowed (%)	9.08
Outlier (%)	0.45

by hydrophobic interactions among residues L27, L31, P66, and L73 of subunit A and residues I165, I166, and V170 of subunit B. Additionally, a hydrogen bond between K30 and Y164 contributes to dimer stabilization (Fig. 2c). By contrast, the interdimer interface displays a non-contacting arrangement, with the closest distance between dimers being approximately 5 Å (e.g., between residues L31 and V170). The K30-Y164 hydrogen bond is disrupted due to the extended distance (5.2 Å), resulting in a loosely packed hexameric channel. While the Derlin-1 dimers serve as the structural units of the hexamer, the non-contacting interface between the dimers indicates that the formation of the overall hexameric channel likely depends on an additional structural foundation, such as its interaction with the p97 hexameric ring. This interaction may provide the necessary stability and organization to maintain the hexameric assembly, compensating for the lack of direct contact between the Derlin-1 dimers.

Comparison between the hexameric channel and Derlin-1 tetramer

As illustrated in Fig. 3a, structural comparisons of the two subunits within a Derlin-1 dimer from the Der-p97 6:6 complex with the Derlin-1 subunits from the Der-p97 4:6 complex in states A and U revealed similar overall folding, with root-mean-square deviations (RMSDs) of 1.4 Å (between subunits A and B in the Derlin-1 dimer 6:6), 2.2 Å (6:6 vs. 4:6, state A), and 3.9 Å (6:6 vs. 4:6, state U). These differences indicate substantial conformational changes within the same protein, primarily localized to transmembrane helices H1, H2, and H6, as well as the loop connecting H1 and H2 (loop$^{1/2}$) (Fig. 3a). The observed variations in the organization of these transmembrane helices enable local conformational adjustments without altering the overall architecture of Derlin-1, facilitating the formation of different oligomeric states.

Previous studies of Derlin-1 and its complex with p97 identified a tetrameric channel arrangement, playing a pivotal role in retrotranslocation within the ERAD pathway. The permeation pathway formed by the Derlin-1 tetramer in C2 symmetry has a diameter of 12–15 Å, sufficient for misfolded proteins to pass through (Fig. 3b). In contrast, the Der-p97 6:6 complex features a hexameric Derlin-1 channel in C3 symmetry, forming a substantially larger permeation pathway with a diameter exceeding 36 Å at its narrowest point (Fig. 3b and Supplementary Fig. 3), as estimated using the program HOLE[30]. However, such a large channel is unlikely to be maintained routinely, as it could lead to potential leakage from the ER lumen.

The "U"-shaped Derlin-1 tetramer described in a previous study[29] appears to result from stretching forces exerted by the NTDs of p97, which "tear" the tetrameric channel between the δ and γ subunits. Interestingly, the four subunits in this conformation occupy four adjacent vertices of a near-regular hexagon, resembling a hexamer missing two subunits. This observation suggests that the hexameric channel might be formed by incorporating a Derlin-1 dimer into the "U"-shaped Derlin-1 tetramer. Structural comparisons between the Der-p97 6:6 and 4:6 (state U) complexes show a largely conserved arrangement of Derlin-1 subunits atop p97 (Fig. 2b). When aligned using the p97 ring as a reference, the Derlin-1 tetramer in 4:6 (state U) is positioned in the same plane as the Derlin-1 hexamer in 6:6, with no significant tilting (Fig. 2b, inset).

Despite these similarities, significant differences are observed in the interfaces between Derlin-1 subunits. While the overall location and orientation of the Derlin-1 subunits are similar in a superposition using the p97 ring as a reference (Fig. 2b), the intradimer interface in the Derlin-1 hexamer exhibits tighter interactions than those observed in the "U"-shaped Derlin-1 tetramer (Fig. 2d). To experimentally test the role of residues identified at the Derlin-1 intradimer interface, we introduced targeted mutations and assessed their impact on dimer formation using chemical crosslinking in HEK293T cells. The mutations on the hydrophobic residues at the intradimer interface, such as V170A and L31A, decreased the intensity of these crosslinked dimers in SDS-PAGEs (Supplementary Figs. 4 and 11), suggesting that mutations of these key hydrophobic residues effectively disrupt Derlin-1 dimerization in cellular contexts.

When superimposed using one Derlin-1 subunit within the interface as the reference, the neighboring subunits in the hexameric channel and the "U"-shaped tetramer display a non-contacting but distinct spatial arrangement (Fig. 2e). In the "U"-shaped tetramer, the geometric relationships among the four subunits exhibit an included angle of approximately 65°–80° between neighboring Derlin-1 subunits. In the hexamer, the included angle between Derlin-1 subunits in adjacent dimers is approximately 30°, which is offset by the ~90° included angle between the subunits within each dimer. This results in an approximate 90° - 30° = 60° rotation between every other Derlin-1 subunit in the hexamer (Supplementary Fig. 5). In summary, while the hexameric Derlin-1 channel maintains an overall subunit arrangement on the p97 ring similar to the "U"-shaped tetrameric channel in the 4:6 complex (state U), the individual orientation and helices conformation of the Derlin-1 subunits differ. These structural differences enable the hexamer to adopt a hexagonal geometry consistent with C3 symmetry, thereby supporting its distinct functional and structural roles in ERAD.

The p97 subunits in Der-p97 6:6 complex

The non-contacting organization of Derlin-1 dimers within the hexameric channel suggests that an additional structural factor is required to maintain the three dimers in a C3 symmetry configuration. Previous studies have shown that the p97 NTD associates with the SHP motif at the C-terminal region of Derlin-1, with this interaction reciprocally influencing the

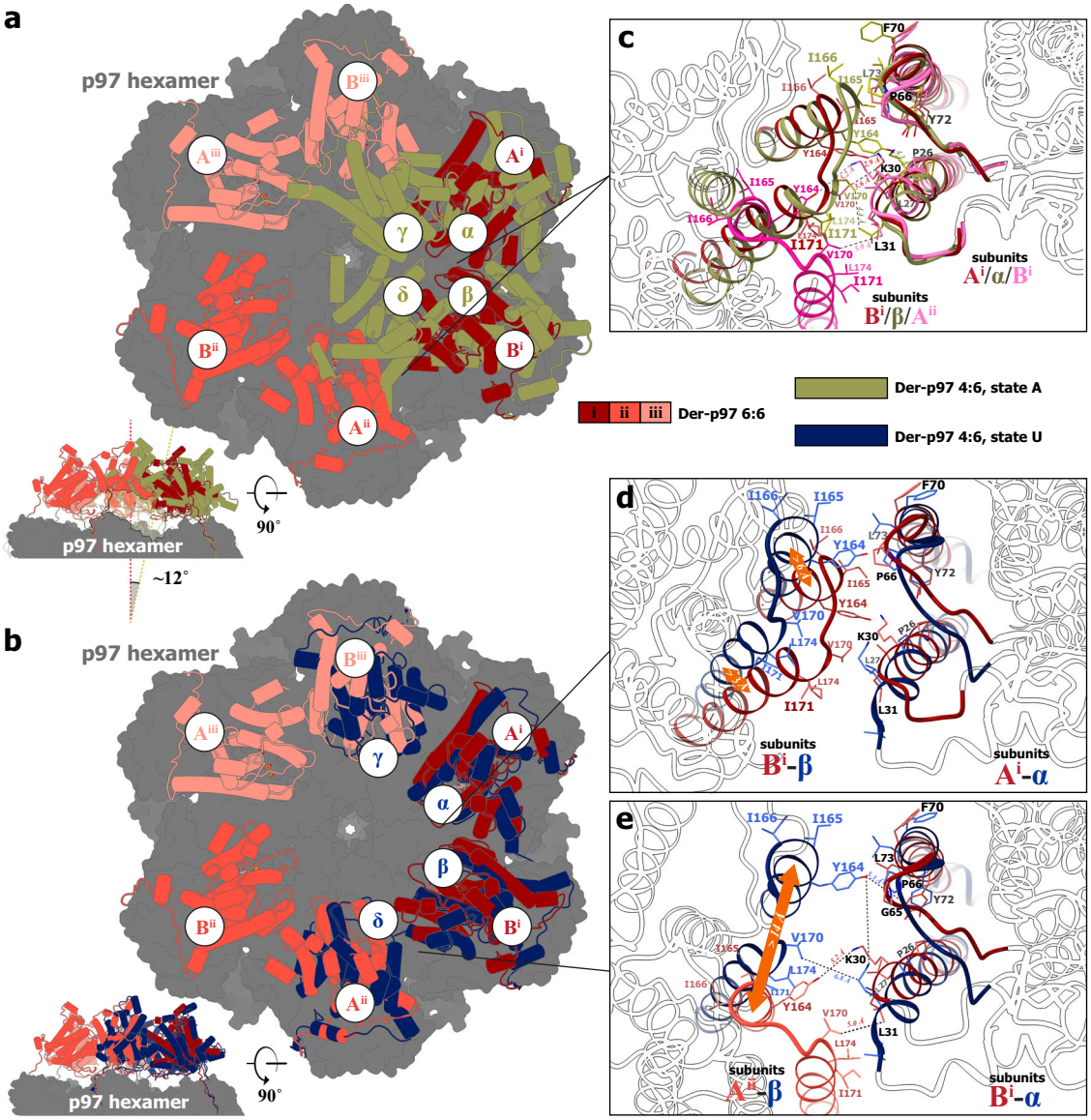

Fig. 2 | The Derlin-1 in hexameric, tetrameric "U"-shaped, and tetrameric channel conformations. a Comparison of the Der-p97 6:6 and 4:6 complexes (state A). The structural model of the Der-p97 6:6 complex was superposed with the Der-p97 4:6 complex in state A (PDB ID 7Y53) using the p97 hexamer as the reference. The p97 hexamer is shown as a surface model in gray. The Derlin-1 subunits are represented as cartoon models, with those from the 4:6 complex colored in yellow and the dimers (i, ii, iii) from the 6:6 complex colored in dark red, red, and pink-red, respectively. **b** Comparison of the Der-p97 6:6 and 4:6 complexes (state U). The structural model of the Der-p97 6:6 complex was superposed with the Der-p97 4:6 complex in state U (PDB ID 7Y59) using the p97 hexamer as the reference. The Derlin-1 subunits from the 4:6 complex (state U) are colored in blue, and the Derlin-1 dimers (i, ii, iii) in the 6:6 complex are colored in dark red, red, and pink-red, respectively. **c** Comparison of dimeric interfaces within Derlin-1 channels. The Derlin-1 subunits A^i/B^i in the 6:6 complex were superposed with subunits B^i/A^{ii} from the same 6:6 complex and subunits α/β from the 4:6 complex in state A (PDB ID 7Y53). The structural models are displayed as cartoon models, with helices and loops involved in the dimeric interfaces highlighted in red for the intradimer interface (A^i/B^i), pink for the interdimer interface (B^i/A^{ii}), and yellow for the tetrameric interface (α/β). **d** Comparison of intradimer interfaces between the 6:6 complex and state U of the 4:6 complex. The Derlin-1 subunits A^i/B^i in the 6:6 complex were superposed with subunits α/β in the 4:6 complex in state U (PDB ID 7Y59) using A^i and α as the reference. The structural models are shown as cartoon models, with helices and loops involved in the dimeric interfaces highlighted in red for the intradimer interface (A^i/B^i) and blue for the tetrameric interface in state U (α/β). **e** Comparison of interdimer interfaces between the 6:6 complex and state U of the 4:6 complex. The Derlin-1 subunits B^i/A^{ii} in the 6:6 complex were superposed with subunits α/β in the 4:6 complex in state U (PDB ID 7Y59) using B^i and α as the reference. The structural models are shown as cartoon models, with helices and loops involved in the dimeric interfaces highlighted in red for the interdimer interface (A^i/B^i) and blue for the tetrameric interface in state U (α/β).

conformations of both p97 and Derlin-1. Depending on the degree of displacement of the p97 NTD relative to its main body and the D2 domain, p97 subunits have been categorized into several conformational states: conformations I and III (conf. I and III) represent the "down" and "up" states of p97 NTD without Derlin-1 binding[31], while conformations C and D (conf. C and D) correspond to two "up" states of p97 NTD bound to Derlin-1[29], with conf. D displaying a higher degree of lifting compared to conf. III (Fig. 4a, b). In the Der-p97 6:6 complex, all six $p97^{NTD}$ adopt a similar conformation, where they are elevated above conf. I and occupy an intermediate position between conf. I and III (Fig. 4a, b). Structural superposition analysis revealed that the Derlin-1-engaging $p97^{NTD}$ in the 4:6 complex (state U) adopts a conformation closely resembling the NTD conformation observed in the 6:6 complex (Fig. 4b, c). This new state, designated as conf. IV, represents a distinct conformation of p97, highlighting its structural flexibility in mediating ERAD retrotranslocation via the Derlin-1 channel.

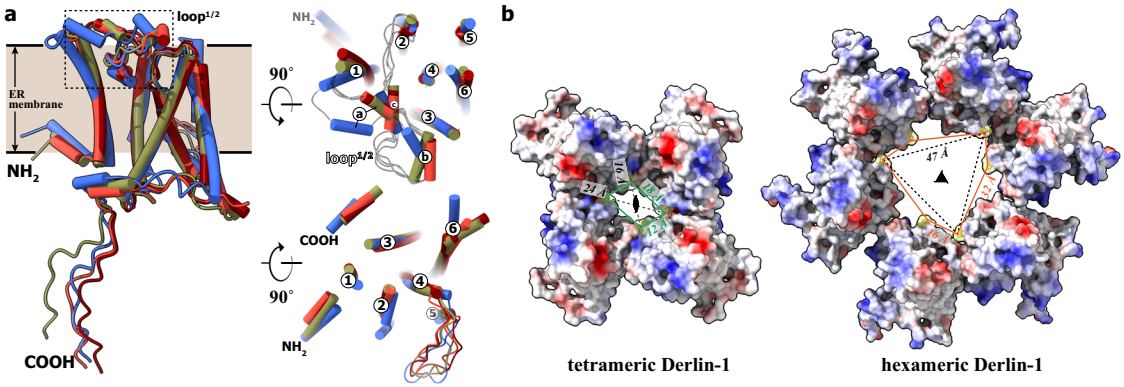

Fig. 3 | The conformational flexibility of Derlin-1. a Structural comparison of Derlin-1 protomers in different states. The structural models of Derlin-1 protomers from the hexameric channel (red), the tetrameric channel (4:6 complex state A, yellow), and the "U"-shaped tetrameric states (4:6 complex state U, blue) are displayed as cartoon models and viewed from three distinct angles to illustrate their conformational flexibility. **b** Central tunnel architecture of tetrameric and hexameric Derlin-1 channels. The central tunnels formed by the tetrameric Derlin-1 channel (left, 4:6 complex state A) and the hexameric Derlin-1 channel (right, 6:6 complex) are shown as electrostatic surface potential maps. The P66 residues, which define the narrowest point of the tunnel, are rendered as transparent to highlight the channel pathways.

Discussion

The retrotranslocation pathway for misfolded proteins from the ER lumen to the cytoplasm, where the proteasome degrades them, remains a critical yet unresolved question in ERAD research. Proposed molecular systems for this process include the oligomeric Derlin channel[20,29], the Hrd1 hemichannel[32] or Hrd1-Der1 complex[23], and Sec61 proteins[33]. Among these, the human Derlin-1 channel is particularly notable due to its wide trans-ER membrane tunnel and its interaction with the ATPase p97, which provides the energy necessary for retrotranslocation, making it a central component in misfolded protein transport machinery. Previous structural studies have highlighted the structural flexibility of the Derlin-1 channel, including the identification of a "U"-shaped conformation with a large opening facing the surrounding lipid bilayer. This open conformation allows the recruitment of misfolded proteins or other ERAD factors, particularly membrane-bound ones, into the Derlin-1/p97 complex. However, the identities of the proteins captured by this "U"-shaped conformation remain unknown.

In this study, instead of identifying a third protein factor in the "U"-shaped Der-p97 4:6 complex, we discovered that Derlin-1 itself can occupy the opening formed by this conformation, assembling into a hexameric channel of significantly larger size. In this configuration, Derlin-1 forms structural dimers, and the non-contacting interactions between the dimers suggest that hexamer formation is primarily mediated by interactions between Derlin-1 and p97. This hexameric Derlin-1 channel features a substantially wider central tunnel across the ER membrane, which may accommodate the translocation of large ERAD substrates (Fig. 5). However, this finding raises further questions about the formation and regulation of the hexameric channel.

Cryo-EM analysis without p97 shows that human Derlin-1 naturally forms a tetramer in the ER membrane, raising questions about how the dimeric unit in the hexameric Derlin-1 is generated. It remains unclear whether the dimeric form exists stably in the ER membrane or is produced by the "tearing" of a tetramer into halves by p97, as suggested by the "U"-shaped conformation. It is an essential question about how p97's nucleotide state influences Derlin-1 oligomerization. However, there are inherent technical challenges in capturing such transitions by cryo-EM. The formation of the 6:6 complex likely requires the incorporation of an additional Derlin-1 dimer into the side-open (U-shaped) 4:6 complex. However, once solubilized in detergent micelles during purification, each Derlin-1/p97 complex becomes sequestered in an individual micelle, effectively isolating complexes and preventing the inter-complex exchange of Derlin-1 subunits. As a result, the 4:6-to-6:6 transition is physically restricted after extraction from membranes. Although we added nucleotides prior to solubilization, it is likely that longer incubation or membrane-reconstituted systems would be needed to promote full conformational maturation (Supplementary Fig. 6).

The apparent dependence of the 6:6 complex abundance on nucleotide ligands in cryo-EM analysis suggests that the ATPase activity of p97 may be crucial for hexameric channel formation. Our cryo-EM analysis showed that the 6:6 complex is predominantly stabilized under ADP·BeF_x conditions, indicating a nucleotide-dependent and likely transient state. ATP-bound p97 favors the side-open U-shaped 4:6 complex, while ADP-bound p97 stabilizes more closed tetrameric and hexameric conformations. Although we have not directly visualized substrate binding, these observations suggest the conformational switch correlates with functional stages of retrotranslocation. Additionally, the large central tunnel (~36 Å) formed in the Derlin-1 hexamer raises concerns about membrane permeability. However, cryo-EM maps reveal unmodeled, elongated densities within the central tunnel, which may correspond to embedded phospholipids or substrate transmembrane segments (Supplementary Fig. 7). These findings suggest that the pore is not hollow but at least partially occluded under physiological or experimental conditions, thereby reducing the risk of membrane leakage. Due to the limited resolution in this region, we did not model specific lipid species; however, the observed densities are consistent with a lipid- or substrate-filled architecture. Despite these insights, it remains uncertain whether the Derlin-1/p97 complex adopts the 4:6 or 6:6 configuration under physiological conditions in the native ER membrane. Further studies, including in situ imaging and native membrane reconstitution, will be needed to distinguish 4:6 and 6:6 complexes under physiological conditions.

To further validate our structural findings, we utilized AlphaFold3 (AF3) modeling to examine the intrinsic oligomerization potential of Derlin-1. AF3 accurately predicted a tetrameric channel consistent with our 4:6 complex structure. In contrast, when modeling a hexameric state, AF3 did not generate a closed ring but instead suggested a dual-trimeric architecture, indicating that Derlin-1 alone lacks a strong propensity to form a stable hexameric channel (Supplementary Fig. 8). Notably, concatenating six Derlin-1 sequences in tandem to mimic spatial constraints imposed by p97 yielded a hexamer-like assembly, albeit differing from the cryo-EM observed structure. These results are consistent with our structural analysis and support the notion that p97 acts as a scaffold, organizing and stabilizing the 6:6 Derlin-1/p97 complex rather than it forming spontaneously.

Although the hexameric Derlin-1/p97 complex likely accommodates bulky substrates, directly linking distinct structural states to specific functional roles in ERAD remains challenging and largely speculative. Testing the functional role of the 6:6 assembly—such as effects on substrate

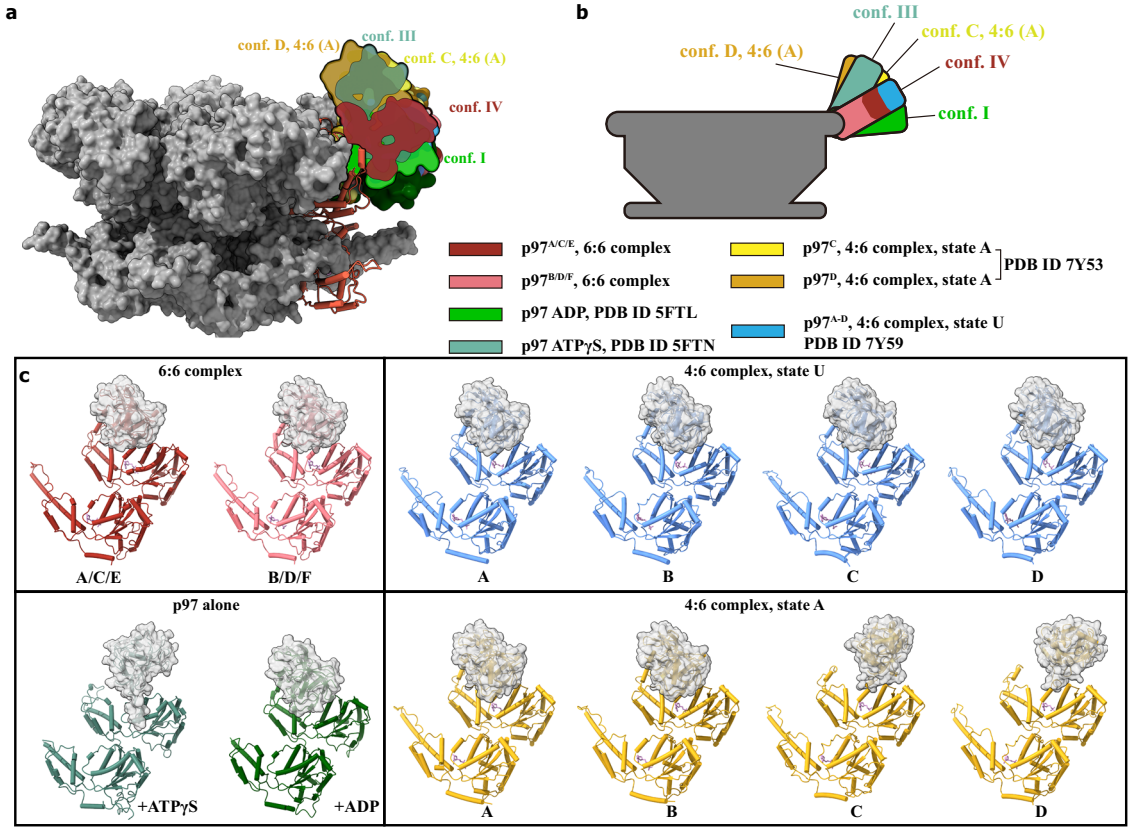

Fig. 4 | The NTD of p97 in different states. a Comparison of $p97^{NTD}$ in different conformations. The p97 protomers from the p97-ADP complex, p97-ATPγS complex, Der-p97 6:6 complex, and Der-p97 4:6 complex in state A and U were structurally aligned using the D1-D2 domain as reference. Their NTDs were shown as surface model and colored in red (for protomers A/C/E from 6:6 complex), pink (for protomers B/D/F from 6:6 complex), light yellow (for protomer C from 4:6 complex, state A), dark yellow (for protomer D from 4:6 complex, state A), light green (for p97-ADP complex), dark green (for p97-ATPγS complex), and blue (for 4:6 complex, state U). The surface models of $p97^{NTD}$ were sliced for a clear observation of their lifting angles. **b** The cartoon representations of the p97 NTD conformations in (**a**). **c** The p97 protomers in different complexes.

selectivity or p97 ATPase regulation—requires precise in vitro assays. However, the structural complexity and overlapping interfaces between tetrameric and hexameric states make it difficult to design mutations that specifically disrupt the 6:6 state without affecting others, complicating functional dissection. Despite these challenges, functional validation remains essential to clarify the biological roles of the observed conformations. Our structural data provide a foundation for future targeted mutations and assays to explore Derlin-1/p97 dynamics. In the ER membrane environment, the Derlin-1/p97 complex may exist in multiple conformational and oligomeric states. Further studies, including in situ imaging and native membrane reconstitution, will be needed to distinguish 4:6 and 6:6 complexes under physiological conditions.

In addition to the nucleotide state of p97, other ERAD partner proteins may also influence the assembly and conformational states of the Derlin-1/p97 complex. Structural comparisons suggest that cofactors such as UFD1/NPL4 are likely compatible with the open 4:6 conformation but may sterically hinder the formation of the closed 6:6 state. Similarly, membrane-bound factors like HRD1 and SEL1L could, in principle, limit the structural rearrangements required for hexamer formation. Other modulators such as UBXD1, known to affect p97 ATPase activity, might indirectly influence Derlin-1 oligomerization dynamics (Supplementary Fig. 9). Together, these possibilities raise the prospect that ERAD cofactors contribute to the conformational regulation of the Derlin-1/p97 complex.

In summary, our findings reveal that the intrinsic hexamerization tendency of p97 mediates the degree of polymerization of the Derlin-1 channel. Derlin-1 can form tetrameric or hexameric channels, as well as a side-open "U"-shaped conformation. This highlights the dynamic and modular nature of the Derlin-1/p97 complex, where interactions with p97 dictate the assembly and function of the Derlin-1 channel. These insights provide a framework for further investigation into the structural and functional versatility of ERAD machinery.

Methods

Protein expression and purification

The cDNA encoding truncated human Derlin-1 (UniProt ID: Q9BUN8) with a 25-amino acid deletion (residues 215-239) was cloned into a pFastBac Dual vector under the control of the polyhedrin promoter, incorporating a PreScission Protease cleavage site and a carboxy-terminal twin strep tag. The cDNA encoding truncated human p97 (UniProt ID: P55072) with the deletion of amino acid residues 1–20 was cloned into the same vector under the control of the P10 promoter. The primer sequences used for these constructs are listed in Supplementary Table 1. The Derlin-1/p97 complex was expressed and affinity-purified as described previously[29] from *Spodoptera frugiperda* (Sf9) cells.

Recombinant baculoviruses were generated using the Bac-to-Bac system (Invitrogen). Sf9 cells were cultured in ESF 921 Insect Cell Culture Medium at 27 °C with shaking at 110 rpm and infected with recombinant baculoviruses at a cell density of $2.5–3 \times 10^6$ cells/mL. After 72 h of infection, cells were harvested by centrifugation at $1500 \times g$ for 15 min and resuspended in lysis buffer containing 20 mM HEPES (pH 7.5), 150 mM NaCl, 10% glycerol, 10 mM $MgCl_2$, 0.2 mg/mL DNase I, and 1× protease inhibitor cocktail (MCE), supplemented with 1 mM ATP·BeF_x or 1 mM ADP·BeF_x, or without any nucleotide ligands. The resuspended cells were lysed by

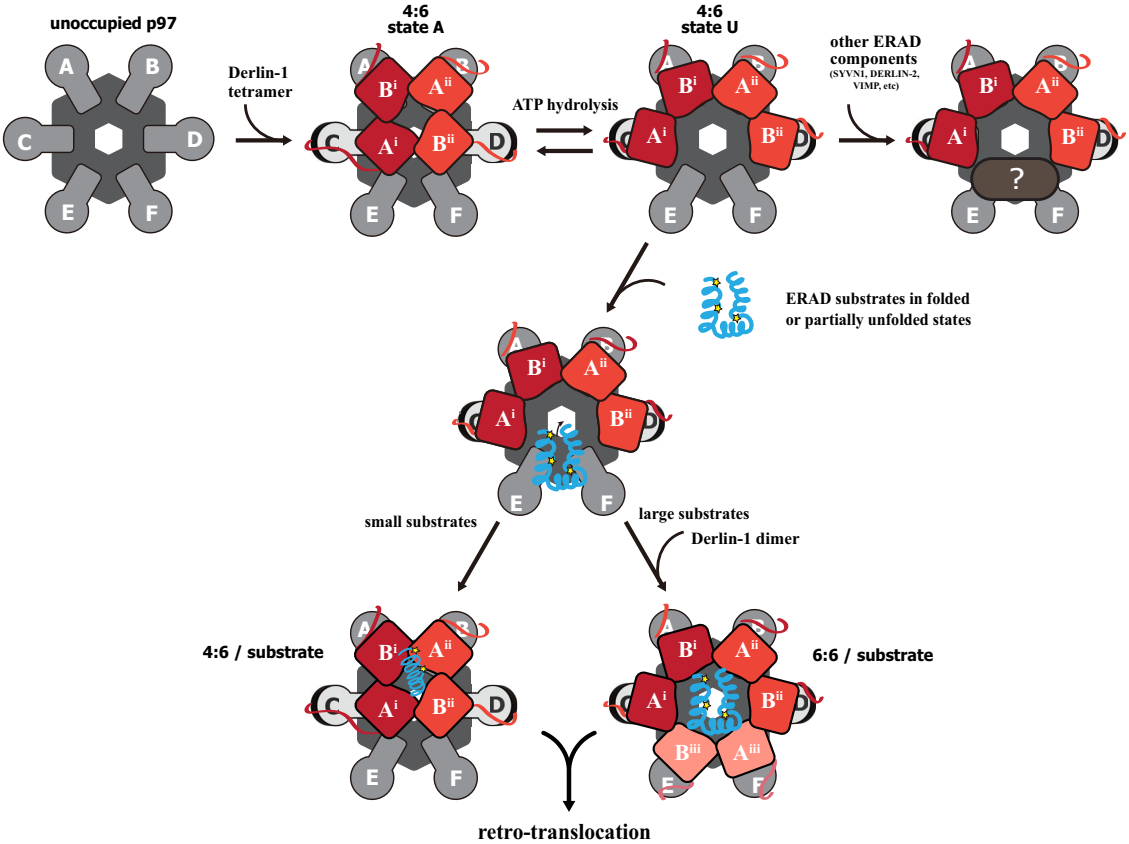

Fig. 5 | A schematic diagram illustrating the proposed transitions. During ERAD, p97 associates with Derlin-1 tetramers to form a 4:6 complex, which can adopt either a closed (state A) or a side-open (state U) conformation. Depending on substrate size and nucleotide state, the complex either accommodates small substrates directly or recruits an additional Derlin-1 dimer to form the 6:6 assembly, thereby enabling retrotranslocation of larger substrates.

sonication on ice, and the lysate was solubilized with 1% (w/v) lauryl maltose neopentyl glycol (LMNG; Anatrace) at 4 °C for 2 h. Following solubilization, the lysate was centrifuged at 46,000 × *g* for 45 min at 4 °C. The supernatant containing the solubilized complex was incubated with Strep-Tactin resin (IBA) for 2 h at 4 °C. The resin was washed with 20 column volumes of wash buffer containing 20 mM HEPES (pH 7.5), 150 mM NaCl, 10% glycerol, and 0.04% glyco-diosgenin (GDN), supplemented with 1 mM ATP·BeFx or 1 mM ADP·BeFx, or without any nucleotide ligand. The complex was eluted with elution buffer containing 20 mM HEPES (pH 7.5), 150 mM NaCl, 10% glycerol, 0.04% GDN, and 5 mM D-desthiobiotin, supplemented with 1 mM ATP·BeF_x or 1 mM ADP·BeF_x, or without any nucleotide ligand. The eluted sample was concentrated and further purified by size-exclusion chromatography on a Superose 6 Increase 10/300 GL column (GE Healthcare) pre-equilibrated with 20 mM HEPES (pH 7.5), 150 mM NaCl, and 0.02% GDN, supplemented with either 1 mM ATP·BeF_x or 1 mM ADP·BeF_x, or no nucleotide ligands, depending on the experimental condition. The purified complex was concentrated to approximately 15 mg/mL for cryo-EM sample preparation.

Cryo-EM sample preparation and data collection

For cryo-EM grid preparation, 3 µL aliquots of the truncated Derlin-1/p97 complex were applied to glow-discharged holey carbon grids (Quantifoil R1.2/1.3 Au, 300 mesh). The grids were blotted using a Vitrobot Mark IV (FEI) and rapidly plunged into liquid ethane for vitrification. The grids were then transferred to a 300 kV Titan Krios transmission electron microscope (FEI) for imaging. Cryo-EM data were collected using a K3 camera (Gatan) at a nominal magnification of 81,000×, corresponding to a pixel size of 1.1 Å on the object scale. Images were acquired in super-resolution mode with a defocus range of −1.0 to −2.5 µm. The accumulated electron dose was set to 50 electrons per $Å^2$, distributed over 32 frames per micrograph.

Cryo-EM data processing

For the Der^{Δ}-$p97^{\Delta}$ ADP·BeF_x dataset, a total of 11,785 movie stacks were collected and subjected to beam-induced motion correction using MotionCor2. The contrast transfer function (CTF) parameters were estimated using Gctf. Low-quality micrographs were removed manually. A total of 5,383,722 particles were automatically picked using Gautomatch-v0.56 (https://www2.mrc-lmb.cam.ac.uk/research/locally-developed-software/zhang-software/#gauto) with fourfold binning, resulting in an initial pixel size of 4.4 Å. Two rounds of reference-free 2D classification were performed in RELION 3.1 to remove junk particles and aggregates. Good particles were then re-extracted at a pixel size of 2.2 Å and imported into cryoSPARC for ab initio model generation, yielding five initial 3D volumes.

After further heterogeneous refinement, particles exhibiting larger Derlin-1 micelle density—presumably corresponding to hexameric Derlin-1—were selectively re-extracted at full resolution (bin1, 1.1 Å/pixel) and subjected to auto-refinement with C3 symmetry imposed. All subsequent steps were carried out with C3 symmetry enforced. A soft mask encompassing the Derlin-1 region was used in two rounds of focused 3D classification to better resolve its conformational heterogeneity. Particles were classified into distinct states based on the number of clearly resolved Derlin-1 protomers visible in the density map. Classes with weak or missing density at certain Derlin-1 positions were excluded from further processing. Ultimately, a subset of 129,127 particles containing a complete Derlin-1 hexamer was selected for additional auto-refinement, Bayesian polishing, and CTF refinement. A 3.55 Å map was obtained based on the gold-standard Fourier shell correlation (FSC) 0.143 criterion. The local resolution ranged from 2.7 to 5.5 Å. (Supplementary Figs. 2 and 10, Table 1).

Model building and refinement

The cryo-EM structure model of the human Derlin-1/p97 complex (PDB ID: 7Y59) was used as a reference for initial model building in Phenix[34]. The initial model was docked into the electron density map using UCSF ChimeraX[35], and subsequently refined through iterative manual adjustments in COOT[36] and real space refinement in Phenix. All the structure-related figures were prepared in UCSF ChimeraX[35].

Cell culture, transfections, and immunoblotting

HEK293T cells were cultured in Dulbecco's modified Eagle's medium (DMEM; Sigma-Aldrich) supplemented with 10% fetal bovine serum (FBS; Wisent Corporation, catalogue # 080-150) at 37 °C in a humidified incubator with 5% CO_2. Cells were seeded in 6-well plates and transfected at ~70–80% confluency with either wild-type or mutant C-terminally Strep-tagged Derlin-1 plasmids using Lipofectamine 2000 (Thermo Fisher Scientific), according to the manufacturer's instructions. After 12 h of transfection, cells were gently washed once with D-PBS, and then incubated with 0.25 mM bismaleimidohexane (BMH; Thermo Fisher Scientific) or 1 mM disuccinimidyl suberate (DSS; Thermo Fisher Scientific) in D-PBS for 10 min at 37 °C to allow cross-linking. Subsequently, the cells were washed again with D-PBS and lysed directly in each well with 200 µL of 5× SDS loading buffer. Lysates were collected and incubated at 95 °C for 10 min, followed by centrifugation at 16,900 × *g* for 10 min at room temperature. The supernatants were collected and analyzed by SDS-PAGE and immunoblotting using standard protocols. Derlin-1 protein was detected using a monoclonal anti-Strep II-Tag antibody (ABclonal, AE066). Western blots were visualized using chemiluminescence detection.

Statistics and reproducibility

Quantitative analysis of Derlin-1 oligomerization was performed by measuring the band intensities of the dimer and monomer forms using ImageJ software (NIH). The intensity ratio between blotting bands corresponding to dimer and monomer was calculated for each sample. Four independent biological replicates were performed per condition. Data were presented as mean ± standard deviation (SD), with individual data points shown where applicable and error bars representing SD.

Reporting summary

Further information on research design is available in the Nature Portfolio Reporting Summary linked to this article.

Data availability

The coordinates are deposited at Protein Data Bank with accession codes: 9LLK. The cryo-EM map has been deposited in the Electron Microscopy Data Bank (EMDB) with accession codes: EMDB-63205. Uncropped and unedited blot images were provided as Supplementary Fig. 11. All data needed to evaluate the conclusions in the paper are present in the paper and/or the Supplementary Information. Unless otherwise stated, all data supporting the results of this study can be found in the article, supplementary, and source data files. Source Data are provided with this paper.

Received: 11 February 2025; Accepted: 11 September 2025;
Published online: 17 October 2025

References

1. Braakman, I. & Hebert, D. N. Protein folding in the endoplasmic reticulum. *Cold Spring Harb. Perspect. Biol.* **5**, a013201 (2013).
2. Werner, E. D., Brodsky, J. L. & McCracken, A. A. Proteasome-dependent endoplasmic reticulum-associated protein degradation: an unconventional route to a familiar fate. *Proc. Natl. Acad. Sci. USA* **93**, 13797–13801 (1996).
3. Posner, B. I. Characterization and modulation of growth hormone and prolactin binding in mouse liver. *Endocrinology* **98**, 645–654 (1976).
4. Christianson, J. C., Jarosch, E. & Sommer, T. Mechanisms of substrate processing during ER-associated protein degradation. *Nat. Rev. Mol. Cell Biol.* **24**, 777–796 (2023).
5. Hwang, J. et al. Characterization of protein complexes of the endoplasmic reticulum-associated degradation E3 ubiquitin ligase Hrd1. *J. Biol. Chem.* **292**, 9104–9116 (2017).
6. Travers, K. J. et al. Functional and genomic analyses reveal an essential coordination between the unfolded protein response and ER-associated degradation. *Cell* **101**, 249–258 (2000).
7. Friedlander, R., Jarosch, E., Urban, J., Volkwein, C. & Sommer, T. A regulatory link between ER-associated protein degradation and the unfolded-protein response. *Nat. Cell Biol.* **2**, 379–384 (2000).
8. Christianson, J. C. et al. Defining human ERAD networks through an integrative mapping strategy. *Nat. Cell Biol.* **14**, 93–105 (2011).
9. Yang, H. et al. Huntingtin interacts with the cue domain of gp78 and inhibits gp78 binding to ubiquitin and p97/VCP. *PLoS ONE***5**, e8905 (2010).
10. Omura, T. et al. A ubiquitin ligase HRD1 promotes the degradation of Pael receptor, a substrate of Parkin. *J. Neurochem.* **99**, 1456–1469 (2006).
11. Tanaka, K., Suzuki, T., Hattori, N. & Mizuno, Y. Ubiquitin, proteasome and parkin. *Biochim. Biophys. Acta* **1695**, 235–247 (2004).
12. Wang, M. & Kaufman, R. J. Protein misfolding in the endoplasmic reticulum as a conduit to human disease. *Nature* **529**, 326–335 (2016).
13. Timms, R. T. et al. Genetic dissection of mammalian ERAD through comparative haploid and CRISPR forward genetic screens. *Nat. Commun.* **7**, 11786 (2016).
14. Lilley, B. N. & Ploegh, H. L. Multiprotein complexes that link dislocation, ubiquitination, and extraction of misfolded proteins from the endoplasmic reticulum membrane. *Proc. Natl. Acad. Sci. USA* **102**, 14296–14301 (2005).
15. Lilley, B. N. & Ploegh, H. L. A membrane protein required for dislocation of misfolded proteins from the ER. *Nature* **429**, 834–840 (2004).
16. Kikkert, M. et al. Human HRD1 is an E3 ubiquitin ligase involved in degradation of proteins from the endoplasmic reticulum. *J. Biol. Chem.* **279**, 3525–3534 (2004).
17. Stolz, A., Hilt, W., Buchberger, A. & Wolf, D. H. Cdc48: a power machine in protein degradation. *Trends Biochem. Sci.* **36**, 515–523 (2011).
18. Ye, Y., Meyer, H. H. & Rapoport, T. A. The AAA ATPase Cdc48/p97 and its partners transport proteins from the ER into the cytosol. *Nature* **414**, 652–656 (2001).
19. Ye, Y., Shibata, Y., Yun, C., Ron, D. & Rapoport, T. A. A membrane protein complex mediates retro-translocation from the ER lumen into the cytosol. *Nature* **429**, 841–847 (2004).
20. Rao, B. et al. The cryo-EM structure of an ERAD protein channel formed by tetrameric human Derlin-1. *Sci. Adv.* **7**. https://doi.org/10.1126/sciadv.abe8591 (2021).
21. Greenblatt, E. J., Olzmann, J. A. & Kopito, R. R. Derlin-1 is a rhomboid pseudoprotease required for the dislocation of mutant alpha-1 antitrypsin from the endoplasmic reticulum. *Nat. Struct. Mol. Biol.* **18**, 1147–1152 (2011).
22. Nejatfard, A. et al. Derlin rhomboid pseudoproteases employ substrate engagement and lipid distortion to enable the retrotranslocation of ERAD membrane substrates. *Cell Rep.* **37**, 109840 (2021).
23. Wu, X. et al. Structural basis of ER-associated protein degradation mediated by the Hrd1 ubiquitin ligase complex. *Science* **368**. https://doi.org/10.1126/science.aaz2449 (2020).
24. Vitali, D. G., Fonseca, D. & Carvalho, P. The derlin Dfm1 couples retrotranslocation of a folded protein domain to its proteasomal degradation. *J. Cell Biol.* **223** https://doi.org/10.1083/jcb.202308074 (2024).

25. Neal, S. et al. The Dfm1 Derlin is required for ERAD retrotranslocation of integral membrane proteins. *Mol. Cell* **69**, 306–320 e304 (2018).
26. Mehnert, M., Sommer, T. & Jarosch, E. Der1 promotes movement of misfolded proteins through the endoplasmic reticulum membrane. *Nat. Cell Biol.* **16**, 77–86 (2014).
27. Lim, J. J. et al. Structural insights into the interaction of human p97 N-terminal domain and SHP motif in Derlin-1 rhomboid pseudoprotease. *FEBS Lett.* **590**, 4402–4413 (2016).
28. Rao, B. et al. The cryo-EM structure of the human ERAD retrotranslocation complex. *Sci. Adv*. **9** https://doi.org/10.1126/sciadv.adi5656 (2023).
29. Rao, B. et al. The cryo-EM structure of the human ERAD retrotranslocation complex. *Sci. Adv.* **9**, eadi5656 (2023).
30. Smart, O. S., Neduvelil, J. G., Wang, X., Wallace, B. A. & Sansom, M. S. HOLE: a program for the analysis of the pore dimensions of ion channel structural models. *J. Mol. Graph* **14**, 354–360, 376 (1996).
31. Banerjee, S. et al. 2.3 A resolution cryo-EM structure of human p97 and mechanism of allosteric inhibition. *Science* **351**, 871–875 (2016).
32. Schoebel, S. et al. Cryo-EM structure of the protein-conducting ERAD channel Hrd1 in complex with Hrd3. *Nature* **548**, 352–355 (2017).
33. Wiertz, E. J. et al. Sec61-mediated transfer of a membrane protein from the endoplasmic reticulum to the proteasome for destruction. *Nature* **384**, 432–438 (1996).
34. Liebschner, D. et al. Macromolecular structure determination using X-rays, neutrons and electrons: recent developments in Phenix. *Acta Crystallogr D. Struct. Biol.* **75**, 861–877 (2019).
35. Pettersen, E. F. et al. UCSF ChimeraX: structure visualization for researchers, educators, and developers. *Protein Sci.* **30**, 70–82 (2021).
36. Emsley, P., Lohkamp, B., Scott, W. G. & Cowtan, K. Features and development of Coot. *Acta Crystallogr. D. Biol. Crystallogr.* **66**, 486–501 (2010).

Acknowledgements

The authors thank Drs. Ming Lei and Lijun Wang for scientific discussion. This work was supported by the National Natural Science Foundation of China (82272519 and 82072468, Y. C.; 82372430, A. Q.), the Shanghai Key Laboratory of Orthopedic Implants (KFKT202207, A. Q.), and the Shanghai Municipal Committee of Science and Technology (20S11902000, Y. C.). This work was also supported by the Shanghai Frontiers Science Center of Degeneration and Regeneration in Skeletal System and the Innovative Research Team of High-level Local Universities (SHSMU-ZLCX20211700, Y. C.) from the Shanghai Municipal Education Commission. W. L. receives the postdoctoral fund from the Ninth People's Hospital, Shanghai Jiao Tong University School of Medicine. We thank the staff members of the Electron Microimaging Center, Bioimaging Facility, and Proteomics Platform at Shanghai Institute of Precision Medicine for providing technical support and assistance in data collection.

Author contributions

Y. C. conceived the study. Y. C., Q. W., B. R., and A. Q. designed the experiments. Q. W., B. R., and Y. X. performed the protein purification and biochemical assays. Q. W., B. R., M. C., Y. S., S. L., and Y. C. performed structural biology experiments. Y. C. and D. Y. built and refined structural models. Y. C., Q. W., and D. Y. wrote the manuscript.

Competing interests

The authors declare no competing interests.

Additional information

Supplementary information The online version contains supplementary material available at https://doi.org/10.1038/s42003-025-08880-5.

Correspondence and requests for materials should be addressed to Yu Cao.

Peer review information *Communications Biology* thanks Zai-Rong Zhang, Chihong Song, and the other, anonymous, reviewer for their contribution to the peer review of this work. Primary Handling Editors: Kaliya Georgieva. A peer review file is available.